Published in final edited form as:
Development. 2009 February ; 136(4): 637–645. doi:10.1242/dev.028621.

Rostral and caudal pharyngeal arches share a common neural crest ground pattern

Maryline Minoux[1,*], **Gregory S. Antonarakis**[2,*], **Marie Kmita**[2,3], **Denis Duboule**[2,4,†], and **Filippo M. Rijli**[1,5,†]

[1]Institut de Génétique et de Biologie Moléculaire et Cellulaire, CNRS/INSERM/ULP, UMR 7104, Strasbourg, France [2]Department of Zoology and Animal Biology and National Research Centre Frontiers in Genetics, University of Geneva, Switzerland [3]Laboratory of Genetics and Development, Institut de Recherches Cliniques de Montréal (IRCM), 110 avenue des Pins Ouest, H2W1R7, Montréal Quebec, Canada [4]School of Life Sciences, Ecole Polytechnique Fédérale, Lausanne, Switzerland [5]Friedrich Miescher Institute for Biomedical Research, Maulbeerstrasse 66, CH-4058 Basel, Switzerland

Abstract

In vertebrates, face and throat structures, such as jaw, hyoid and thyroid cartilages develop from a rostrocaudal metameric series of pharyngeal arches, colonized by cranial neural crest cells (NCCs). Colinear Hox gene expression patterns underlie arch specific morphologies, with the exception of the first (mandibular) arch, which is devoid of any Hox gene activity. We have previously shown that the first and second (hyoid) arches share a common, Hox-free, patterning program. However, whether or not more posterior pharyngeal arch neural crest derivatives are also patterned on the top of the same ground-state remained an unanswered question. Here, we show that the simultaneous inactivation of all Hoxa cluster genes in NCCs leads to multiple jaw and first arch-like structures, partially replacing second, third and fourth arch derivatives, suggesting that rostral and caudal arches share the same mandibular arch-like ground patterning program. The additional inactivation of the Hoxd cluster did not significantly enhance such a homeotic phenotype, thus indicating a preponderant role of Hoxa genes in patterning skeletogenic NCCs. Moreover, we found that *Hoxa2* and *Hoxa3* act synergistically to pattern third and fourth arch derivatives. These results provide insights into how facial and throat structures are assembled during development, and have implications for the evolution of the pharyngeal region of the vertebrate head.

Keywords

Hox genes; Head morphogenesis; Hyoid bone; Jaw development; Mouse; Neural crest cells

[†]Authors for correspondence (denis.duboule@zoo.unige.ch; filippo.rijli@fmi.ch).
[*]These authors contributed equally to this work

Supplementary material
Supplementary material for this article is available at http://dev.biologists.org/cgi/content/full/136/4/637/DC1

INTRODUCTION

A large part of the vertebrate craniofacial skeleton and the entire pharyngeal skeleton derive from cranial neural crest cells (NCCs) that arise along the dorsal edge of the forming neural tube (Creuzet et al., 2005). Cranial NCCs originating from rostral brain regions migrate into the frontonasal process, whereas at hindbrain level, NCCs migrate out of the segmented rhombomeres (R) and colonize the pharyngeal arches (PAs), another series of metameric structures that give rise to maxillary, mandibular, middle ear, hyoid and neck bones (Santagati and Rijli, 2003). Therefore, a segmental pattern underlies the development and morphogenesis of the pharyngeal region of the vertebrate head (Graham, 2007; Kuratani et al., 1997). Nonetheless, fundamental differences exist in the deployment and contribution of NCCs to the PAs between pre-otic (R1–R4) and post-otic (R6–R8) regions.

At pre-otic level, NCCs migrate into separate streams: NCCs from the posterior mesencephalon, R1 and R2 fill the first (mandibular) arch, whereas the second (hyoid) arch is colonized by NCCs originating mainly from R4 (Lumsden et al., 1991; Sechrist et al., 1993). As both R3 and R5 provide little if any NCC contribution to PA derivatives (Graham et al., 1993; Sechrist et al., 1993), this leads to the segregation of first, second and post-otic arch NCCs into distinct streams. By contrast, within post-otic NCCs, there is no segmental registration between their rhombomeric origin and PA contribution (Shigetani et al., 1995), such that NCC subpopulations entering arches 3, 4 and 6 are generated from the entire rostrocaudal extent of the post-otic hindbrain and are partially overlapping, although arch 3 mainly contains NCCs of R6 origin (Shigetani et al., 1995). Such a distribution is also reflected in the overlapping deployment of post-otic NCCs to form skeletal elements of multi-rhombomeric origin, whereas pre-otic NCC sub-populations maintain strict segregation on skeletal derivatives of the first two arches according to their rhombomeric origin (Kontges and Lumsden, 1996). It is therefore unclear whether first and second arches are patterned by molecular mechanisms distinct from those acting in more posterior arches, or whether all PAs belong to a homology series sharing a common ground patterning program.

At the molecular level, NCC subpopulations contributing to distinct PAs express various combinations of Hox genes, providing each arch with distinct regional identities along the anteroposterior (AP) axis (Santagati and Rijli, 2003; Trainor and Krumlauf, 2001). *Hoxa2* is the only Hox gene expressed in the skeletogenic NCCs of the second PA, whereas first arch NCCs are Hox-negative (Couly et al., 1998). In mouse, the inactivation of *Hoxa2* in NCCs resulted in homeotic transformation of second arch derivatives into morphologies characteristic of Hox-negative first arch-derived structures (Gendron-Maguire et al., 1993; Rijli et al., 1993; Santagati et al., 2005). Therefore, *Hoxa2* promotes second arch skeletal development by modifying an underlying Hox-negative, first arch-like ground (default) patterning program, shared by the skeletogenic NCCs of the first and second arches (Rijli et al., 1993). Such a proposal has been further supported by functional studies in other vertebrate systems, including zebrafish, *Xenopus* and chick (Baltzinger et al., 2005; Crump et al., 2006; Grammatopoulos et al., 2000; Hunter and Prince, 2002; Miller et al., 2004; Pasqualetti et al., 2000).

By contrast, third and fourth arch NCC-derived skeletal structures were not affected in *Hoxa2*$^{-/-}$ or *Hoxb2*$^{-/-}$ single or compound mutants (Barrow and Capecchi, 1996; Davenne et al., 1999; Gendron-Maguire et al., 1993; Rijli et al., 1993), suggesting that paralog group 2 (PG2) genes are dispensable or functionally compensated by other Hox genes in arches posterior to the second. Indeed, third arch NCCs express both PG2 Hox (*Hoxa2* and *Hoxb2*) and PG3 (*Hoxa3*, *Hoxb3* and *Hoxd3*) genes (see Fig. S1 in the supplementary material). Functional inactivation of *Hoxa3*, in contrast to both *Hoxb3* or *Hoxd3*, resulted in malformations of the greater horn of the hyoid bone and fusions to the thyroid cartilage (Chisaka and Capecchi, 1991). Such defects were exacerbated in *Hoxa3*$^{-/-}$/*Hoxd3*$^{-/-}$ or *Hoxa3*$^{-/-}$/*Hoxb3*$^{-/-}$ mutants, whereas *Hoxb3*$^{-/-}$/*Hoxd3*$^{-/-}$ compound mutants displayed milder defects when compared with single *Hoxa3*$^{-/-}$ mutants (Condie and Capecchi, 1994; Manley and Capecchi, 1997). Consequently, although dose-dependent genetic interactions occur between *Hoxa3*, *Hoxb3* and *Hoxd3*, there is a prevalent role for *Hoxa3* in patterning third arch NCC derivatives. However, no homeotic transformations were observed in any of the described Hox PG3 mutants. Similarly, single or compound PG4 Hox (*Hoxa4*, *Hoxb4*, *Hoxc4* and *Hoxd4*) mutants did not result in any homeosis of NCC derivatives (Boulet and Capecchi, 1996; Horan et al., 1995; Ramirez-Solis et al., 1993). The question thus remained as to whether or not pre-otic NCCs share an underlying patterning program distinct from that of post-otic NCCs. Alternatively, all pharyngeal arch NCC skeletal derivatives may be built on the top of the same Hox ground patterning program, yet posterior to the second arch the observation of this ground-state would necessitate the deletion in cis of Hox genes belonging to multiple groups of paralogy.

To discriminate between these possibilities, we have deleted all Hoxa genes in NCCs and report here evidence for the occurrence of homeotic transformations of third and fourth arch derivatives towards first arch-like Meckel's cartilage morphology, with additional appearance of ectopic first arch-specific membranous bone elements. These results demonstrate that a common Hox-free ground patterning program is shared caudally to the first and second arches, and that *Hoxa2* and *Hoxa3* act synergistically to pattern third and fourth arch NCC derivatives. Moreover, additional deletion of the entire Hoxd cluster in the context of the NCC-specific Hoxa inactivation did not significantly enhance such a homeotic phenotype, but resulted only in an increase of the frequency of ectopic squamosal bones in posterior pharyngeal arches, suggesting a preponderant role of Hoxa genes in patterning skeletogenic NCCs in mammals. We discuss these results both in terms of Hox-mediated pharyngeal arch patterning and from an evolutionary standpoint.

MATERIALS AND METHODS

Stocks of mice and matings

Generation of conventional *Hoxa2* and conditional *Hoxa2*^{flox} mutant alleles has been described previously (Rijli et al., 1993; Ren et al., 2002). Mice mutant for the Hoxd cluster were as reported previously (Zakany et al., 2001). The floxed Hoxa cluster allele was that described by Kmita et al. (Kmita et al., 2005) and the *Wnt1::Cre* mice were those described by Danielian et al. (Danielian et al., 1998). For the generation of mutant fetuses, *Hoxa*$^{flox/+}$/*Hoxd*$^{del/+}$ specimens were intercrossed, with one parent carrying in addition the *Wnt1::Cre*

transgene. The *R4::Cre* and Z/AP reporter transgenic lines have been described previously (Oury et al., 2006; Lobe et al., 1999).

Skeletal preparation

Newborns were skinned and eviscerated. Skeletons were fixed overnight in 95% ethanol and then stained in Alcian Blue (750 μg/ml in 80 ml of 95% ethanol and 20 ml of glacial acetic acid) for at least 24 hours. Skeletons were cleared in 1% KOH overnight and then stained in Alizarin Red (100 μg/ml in 1% KOH) overnight. Further clearance was performed in 20% glycerol/1% KOH. Skeletons were stocked in 50% glycerol/50% water.

In situ hybridization

In situ hybridization on sections and on whole-mount embryos were performed as previously described (Santagati et al., 2005). The following RNA probes were used: *Hoxa2* (Ren et al., 2002), *Hoxb2* (Vesque et al., 1996), *Hoxa3*, *Hoxb3*, *Hoxd3* (Manley and Capecchi, 1997), *Hoxa4*, *Hoxb4*, *Hoxd4* (Gaunt et al., 1989), *CRABP1* (Maden et al., 1992), *Pax1* (Wallin et al., 1996), *Alx4* (Qu et al., 1997), *Pitx1* (Lanctot et al., 1999) and *Barx1* (Tissier-Seta et al., 1995).

Z/AP staining

E15.5 embryos were fixed overnight in 4% paraformaldehyde (PFA), rinsed in phosphate-buffered saline (PBS), equilibrated in 20% sucrose and included in Cryomatrix (Thermo Electron Corporation). Cryostat sections (20 μm) were cut in the frontal plane of the embryo to visualize the great and lesser horns of the hyoid bone. The sections were then fixed for 1 hour in 4% PFA, rinsed in PBS at room temperature and then incubated in PBS at 65°C during 1 hour to inactivate the endogenous AP. After the inactivation, sections were rinsed in a solution of NTMT (NaCl 0.1 M, Tris HCl 0.1 M (pH 9.5), $MgCl_2$ 0.05 M and Tween 20 0.1%). NBT (3.5 μl; Roche 1383213) and 3.5 μl BCIP (Roche 1383221) per ml of NTMT were used for the staining. The sections were rinsed first in water, next in 100% ethanol and mounted onto slides.

Statistical analysis

A Yates' Chi-square test was used to compare the frequency of appearance of each ectopic membranous bone (i.e. supernumerary tympanic, squamosal and dentary bones) between the group formed by *Wnt1::Cre/Hoxa*$^{flox/flox}$ and *Wnt1::Cre/Hoxa*$^{flox/del}$, and the group formed by *Wnt1::Cre/Hoxa*$^{flox/flox}$*/Hoxd*$^{del/+}$ and *Wnt1::Cre/Hoxa*$^{flox/flox}$*/Hoxd*$^{del/del}$ mutant newborns. The analysis were carried out using Statistica 7.1 software package (Statsoft)

RESULTS

Expression of PG2, PG3 and PG4 Hox genes in pharyngeal arches

To analyze Hox gene expression in PAs, we performed whole-mount in situ hybridization on E10.0 mouse embryos using antisense probes for PG2 (*Hoxa2* and *Hoxb2*), PG3 (*Hoxa3*, *Hoxb3* and *Hoxd3*) and PG4 (*Hoxa4*, *Hoxb4* and *Hoxd4*) genes. In addition to arch 2, PG2 Hox genes were strongly expressed in arches 3 and 4 NCCs (see Fig. S1A,B in the

supplementary material). PG3 Hox genes were expressed in the dorsolateral circumpharyngeal (CP) ridge (see Fig. S1C–E in the supplementary material) from which post-otic NCCs stream into each posterior arch (Shigetani et al., 1995). Among PG3 Hox genes, *Hoxa3* was highly expressed in arches 3 and 4 (see Fig. S1C in the supplementary material), whereas *Hoxb3* and *Hoxd3* transcripts were detected at low level and/or in subsets of arch 3 cells and at relatively high levels in arch 4 (see Fig. S1D–E,I in the supplementary material). Interestingly, in keeping with a previous study on human embryos (Vieille-Grosjean et al., 1997), we found that *Hoxa4* and *Hoxb4* were not expressed at significant levels in arches 3 and 4, but only in more posterior regions (see Fig. S1F–G,J in the supplementary material). By contrast, however, we found *Hoxd4* relatively highly expressed in arch 4 NCCs (see Fig. S1H,K in the supplementary material). To summarize, at E10.0, arch 3 mostly expressed *Hoxa2*, *Hoxb2* and *Hoxa3,* whereas *Hoxa2*, *Hoxb2*, *Hoxa3*, *Hoxb3*, *Hoxd3* and *Hoxd4* transcripts were scored in arch 4.

Generation of Hoxa and Hoxd cluster deletions

Given the above Hox expression patterns, we decided to look at the morphogenesis of post-otic NCC skeletal derivatives after deleting the entire Hoxa and Hoxd gene clusters, either separately or in combination. Cre-loxP mediated targeted deletion of the entire Hoxd cluster (Zakany et al., 2001) resulted in $Hoxd^{del/del}$ newborns with no significant defects at the level of NCC-derived skeletal structures (not shown). By contrast, deletion of the entire Hoxa cluster resulted in premature lethality at early to mid-embryonic stages (Kmita et al., 2005), thus preventing the analysis of NCC derived skeletal elements.

To overcome such an early lethality, we conditionally deleted the entire Hoxa cluster in NCCs, based on a previous observation showing that, at least in the case of *Hoxa2*, selective inactivation in NCCs was sufficient to recapitulate the skeletal phenotype of the full inactivation (Santagati et al., 2005). We used a *Wnt1::Cre* transgenic mouse line in which the *Wnt1* promoter drives Cre recombinase expression in NCC progenitors (Danielian et al., 1998) to cross with a conditional $Hoxa^{flox}$ allele (Kmita et al., 2005). *Wnt1::Cre/* $Hoxa^{flox/flox}$ or *Wnt1::Cre/*$Hoxa^{flox/del}$ fetuses survived throughout fetal development, up to birth, similar to *Wnt1::Cre/* $Hoxa^{flox/flox}$/$Hoxd^{del/+}$ or *Wnt1::Cre/*$Hoxa^{flox/flox}$/$Hoxd^{del/del}$ mutant animals. Newborn mutants, however, eventually died within a few hours, and suffered from several skeletal abnormalities (see below). To assess the efficiency of the *Wnt1::Cre* mediated recombination, we carried out whole-mount in situ hybridization on E10.0 mutant embryos. We have previously shown that the *Wnt1::Cre* driver mated to a *Hoxa2* floxed allele efficiently induces lack of *Hoxa2* expression in NCCs (Ren et al., 2002; Santagati et al., 2005). Similarly, we tested the expression of *Hoxa3* in *Wnt1::Cre/* $Hoxa^{flox/del}$ mutant embryos and observed, as expected, a selective loss of *Hoxa3* transcripts from the NCCs contributing to the third and more posterior PAs, whereas the other sites of *Hoxa3* expression were unaffected (see Fig. S2A–D in the supplementary material), thus validating the conditional deletion approach.

Contribution of pre- and post-otic NCCs to the hyoid bone complex

Studies in non-mammalian vertebrates assessed that the hyoid bone complex has a composite origin from both pre-otic and post-otic NCCs (e.g. Kontges and Lumsden, 1996;

Couly et al., 1998). In mammals, the precise contribution of pre- and post-otic NCCs to the mammalian hyoid complex has not been mapped by long-term tracing experiments. It is generally assumed that the lesser horns of the hyoid bone derive from the second, and the greater horns from the third, arch NCCs. Moreover, the prevalent opinion in literature is that second arch pre-otic NCCs contribute to the upper part of the body of the hyoid bone, whereas third arch post-otic NCCs colonize the lower part (Larsen, 1993).

Given the relevance for our present analysis, we set up to define the pre-otic versus post-otic NCC composition of the hyoid bone apparatus in the mouse. To this aim, we mated a previously described *R4::Cre* mouse line (Oury et al., 2006) to the Z/AP transgenic reporter (Lobe et al., 1999). Upon Cre-mediated recombination, the expression of the alkaline phosphatase (*AP*) gene was permanently activated in the pre-otic NCC progenitors specifically emerging from R4 and colonizing the second pharyngeal arch (Fig. 1G; see Fig. S3A,B in the supplementary material). AP staining was present throughout the arch mesenchyme, except in the central mesodermal core (see Fig. S3B in the supplementary material). Conditional inactivation of *Hoxa2* with the *R4::Cre* driver was sufficient to induce the full extent of the *Hoxa2* knockout mutant phenotype (see Fig. S3C–F in the supplementary material). Namely, all second arch-derived skeletal elements, including the lesser horn of the hyoid bone, were absent and replaced by a duplicated set of first arch-like elements in reverse polarity. Altogether, these data strongly indicated that AP^+ cells represent the vast majority of NCC contribution to the second PA, even though minor contributions from R3- and/or R5-derived NCCs could not be ruled out (e.g. Kontges and Lumsden, 1996). By contrast, post-otic NCCs migrating into third and more posterior arches were devoid of reporter gene expression (Fig. 1G, arrow; see Fig. S3A,B in the supplementary material). Thus, mapping the fate of AP^+ versus AP^- mesenchyme on the hyoid complex essentially allows the assessment of the spatial deployment and contribution of pre-otic (i.e. second arch-derived) versus post-otic (i.e. third arch-derived) NCCs.

AP staining of tissue sections at E15.5 revealed that the lesser horn was entirely made of AP^+ NCCs, whereas the greater horn was entirely AP^-, i.e. of post-otic NCC origin (Fig. 1A–C,H). Interestingly, as for the body of the hyoid bone, we found that pre-otic AP^+ and post-otic AP^- NCCs were deployed in a striped pattern (Fig. 1A–C,H). Pre-otic AP^+ NCCs contributed to the central part of the body, as well as to two symmetrical regions articulating with the lesser horns, which abutted the post-otic AP^- greater horn of the hyoid bone. In summary, our data confirm that the lesser horn is a second arch derivative, whereas the greater horn is most likely of third arch origin. In addition, the body of the hyoid bone is a composite of pre-otic and post-otic NCCs that remain segregated in an alternate striped pattern.

Homeosis of second, third and fourth arch derivatives in Hoxa cluster mutant newborns

Newborns lacking the Hoxa cluster in NCCs displayed an absence of the external ear and cleft palate (not shown), much like the original $Hoxa2^{-/-}$ mutants (Gendron-Maguire et al., 1993; Rijli et al., 1993). Moreover, in the second arch, the phenotypes of skeletal derivatives in *Wnt1::Cre/Hoxa*$^{flox/flox}$ (Fig. 2E,F,I,J; Fig. 4B), *Wnt1::Cre/Hoxa*$^{flox/del}$ (Fig. 4C), *Wnt1::Cre/Hoxa*$^{flox/flox}$*/Hoxd*$^{del/+}$ (Fig. 2G,H; Fig. 4D) or *Wnt1::Cre/Hoxa*$^{flox/flox}$*/*

Hoxd$^{del/del}$ (not shown) mutant fetuses were all similar to those observed upon *Hoxa2* inactivation (Fig. 2C,D), as expected from *Hoxa2* being the sole gene expressed in this arch. In particular, the stapes, styloid process and lesser horns of the hyoid bone were absent and were replaced by mirror-image duplications of first arch-like structures, including partially duplicated Meckel's cartilage (MC2), incus (I2), malleus (M2), tympanic (T2) and pterygoid (P2) bones, as well as transformed gonial (G*) and ectopic squamosal (SQ2) bones. Such an outcome at a skeletal level further confirmed the efficiency of our conditional Hoxa cluster deletion.

In addition, however, newborns lacking the Hoxa cluster in NCCs displayed ectopic skeletal elements (compare Fig. 2E,F,I,J and Fig. 4B–D with Fig. 2C,D), observed neither in single *Hoxa2*$^{-/-}$ or *Hoxa3*$^{-/-}$ specimen, nor in compound *Hoxa3*$^{-/-}$/*Hoxd3*$^{-/-}$ mutant animals (Chisaka and Capecchi, 1991; Condie and Capecchi, 1994; Manley and Capecchi, 1997). In all analyzed mutants (see Table S1 in the supplementary material), the greater horn of the hyoid bone (GH) significantly extended dorsally and resembled a partially triplicated Meckel's cartilage (MC3), whereas MC2 extended further ventrally than in single *Hoxa2*$^{-/-}$ specimen (compare Fig. 2E,F with 2C,D). In addition, in some mutants (see Table S1 in the supplementary material), the dorsal end of such ectopic cartilage displayed a morphology resembling an ectopic first arch-like malleus (M3) (Fig. 2E,F).

A significant fraction of *Wnt1::Cre/Hoxa*$^{flox/flox}$ mutants (nine out of 20) also displayed a notable transformation of the thyroid cartilage, which we interpret as a partial quadruplication of Meckel's jaw cartilage (MC4) (Fig. 2I,J; Fig. 3B). In these mutants, the lateral process (LP) of the thyroid cartilage was reduced and transformed into an ectopic cartilage that projected dorsally and fused with the transformed greater horn of the hyoid bone (MC3). Furthermore, in the mutant presented in Fig. 2I,J, the ectopic MC4 and MC3 directly fused with an MC2 that unusually extended ventrally (posteriorly), further supporting their identity as supernumerary jaw cartilages.

The frequency of MC3 or MC4 was not enhanced upon additional deletion of one or two alleles of the Hoxd cluster (see Table S1 in the supplementary material; and not shown). The *Wnt1::Cre/Hoxa*$^{flox/flox}$ or *Wnt1::Cre/Hoxa*$^{flox/flox}$/*Hoxd*$^{del/+}$ mutant newborns that did not bear the ectopic MC4 displayed fusions between hyoid bone and thyroid cartilage (Fig. 2G,H, arrowhead), reminiscent of the *Hoxa3* inactivation phenotype (Chisaka and Capecchi, 1991), whereas *Wnt1::Cre/Hoxa*$^{flox/flox}$/*Hoxd*$^{del/del}$ mutants displayed a reduction of the thyroid cartilage (data not shown), similar to the *Hoxa3*$^{-/-}$/*Hoxd3*$^{-/-}$ double knockout phenotype (Condie and Capecchi, 1994). Conversely, deletion of only one *Hoxa*^{flox} allele in NCCs, in the context of a full Hoxd deletion (*Wnt1::Cre/Hoxa*$^{flox/+}$/*Hoxd*$^{del/del}$) did not result in morphological transformation, neither of the hyoid bone, nor of the thyroid cartilage, but only in mild malformations (not shown), indicating that the remaining copy of *Hoxa*^{flox} allele was sufficient to compensate for the loss of both Hoxd alleles.

Finally, supernumerary ectopic membranous bones also appeared in a fraction of Hoxa and Hoxa/Hoxd deleted mutants (see Table S1 in the supplementary material; Fig. 2G,H; Fig. 4B–D) that were never observed in wild type, *Hoxa2*$^{-/-}$ or *Hoxa3*$^{-/-}$ mutants, nor in double *Hoxa3*$^{-/-}$/*Hoxd3*$^{-/-}$ newborns. Caudal to SQ2, such ectopic elements may reflect a partial

triplication of squamosal bones (SQ3) (Fig. 4C,D). Additional ectopic membranous elements were also present in the proximity of MC3 and M3, respectively, and may thus represent supernumerary dentary (DB2) and tympanic (T3) bones (Fig. 2G,H). Such supernumerary membranous bones were scored with variable occurrence (see Table S1 in the supplementary material) and often only on one side of the mutants, indicating stochastic compensation for the lack of Hoxa genes in NCCs. The deletion of either one or both Hoxd cluster alleles in a Hoxa mutant background did not significantly enhance this phenotype, with the exception of increasing the frequency of the ectopic SQ3 membranous bones (see Table S1 in the supplementary material) (P=0.01 with the Yates' Chi-square test), thus indicating redundancy with Hoxa genes in repressing the formation of this structure in posterior arches.

Altogether, these results strongly suggested that, in the absence of Hoxa genes in NCCs, the third and fourth arch post-otic NCC derived structures partially underwent homeotic transformations into first arch-like morphologies, similar to arch 2 NCCs, thus pointing to a potential common Hox-free ground patterning program shared by NCCs originating from both pre- and post-otic domains.

Molecular changes in Hoxa mutant arches

To assess the status of NCC migratory streams in Hoxa-deleted mutant embryos, we carried out whole-mount in situ hybridization. As a marker for migrating cranial NCCs, we used an antisense probe for cellular retinoic acid-binding protein 1 (*Crabp1*) (Maden et al., 1992) and found no difference in *Crabp1* expression patterns in E9.5 *Wnt1::Cre/Hoxa*$^{flox/flox}$ or *Wnt1::Cre/Hoxa*$^{flox/flox}$*/Hoxd*$^{del/del}$ mutant embryos, when compared with a wild-type specimen (Fig. 5A,B; and not shown). We then assessed the pattern of PA segmentation by analyzing the expression pattern of *Pax1*, which specifically labels the endodermal pharyngeal pouches, from their initial formation until late stages (Wallin et al., 1996). In E10.0 *Wnt1::Cre/Hoxa*$^{flox/flox}$ and *Wnt1::Cre/Hoxa*$^{flox/flox}$*/Hoxd*$^{del/del}$ mutant embryos, *Pax1* was normally expressed in the endoderm of each pharyngeal pouch and no fusions occurred between adjacent arches, when compared with wild-type embryos (Fig. 5C,D; and not shown). From these results, we concluded that the combined deletion of Hoxd genes in all cells and Hoxa genes in NCCs, had altered neither pharyngeal segmentation nor the migration patterns of cranial NCCs.

We next investigated the molecular identity of pharyngeal arch NCCs in *Wnt1::Cre/Hoxa*$^{flox/flox}$ mutant embryos. In E10.5 wild-type embryos, the expression domains of *Pitx*1, a marker of Meckel's cartilage (Lanctot et al., 1999), and *Alx4* are restricted to the first arch (Fig. 5E,H). In *Wnt1::Cre/Hoxa*$^{flox/flox}$ embryos, both *Pitx1* and *Alx4* were ectopically expressed in the second arch, similar to *Hoxa2*$^{-/-}$ mutants (compare Fig. 5F–G,I–J with 5E,H) (Santagati et al., 2005). In addition, however, *Alx4* and *Pitx1* were ectopically expressed either in the third, or in both the third and fourth PAs, respectively, of *Wnt1::Cre/Hoxa*$^{flox/flox}$ mutant embryos (Fig. 5G,J). Notably, the *Pitx1* ectopic expression domains in PA2-4 were confined posteriorly, thus opposite to the wild-type pattern in anterior PA1 (compare Fig. 5E with 5G). This observation might well correlate with the potentially reversed polarity of the ectopic MC3 and MC4 in these mutants, in addition to the mirror-

imaged MC2 expected from the *Hoxa2* deletion in PA2 (Fig. 2E–J). *Barx1*, a marker of chondrocyte differentiation and condensation (Sperber and Dawid, 2008), is expressed in all pharyngeal arches of wild-type embryos, although with arch-specific differences in its spatial distribution (Fig. 5K). Indeed, at E10.5 *Barx1* is highly expressed in the mandibular and maxillary portions of PA1 and in ventral PA2, as well as at lower levels in ventral PA3 and PA4 (Fig. 5K). *Barx1* transcripts are also present in a small domain at the dorsoanterior margin of PA2 (Fig. 5K, arrowhead). In $Hoxa2^{-/-}$ mutant embryos, such domain was extended ventrally and posteriorly (similar to PA1) (Fig. 5L). Similarly, this ectopic *Barx1* domain was also observed in $Wnt1::Cre/Hoxa^{flox/flox}$ mutant PA2 (Fig. 5M, arrow). In addition, an ectopic expression domain of *Barx1* appeared in the dorsal part of PA3 (Fig. 5M, arrow). Altogether, these results further support a view whereby the deletion of the Hoxa cluster in NCCs results, in addition to PA2 molecular changes, in transformation of PA3 and PA4 gene expression patterns into a first arch, jaw-like pattern, thus indicating that post-otic NCCs acquired partial first arch-like identities.

DISCUSSION

This study provides novel insights into the molecular mechanisms underlying craniofacial patterning. We report that the conditional deletion of the Hoxa cluster in NCCs induced a more extensive phenotype than the mere combination of *Hoxa2* and *Hoxa3* loss of functions. In such conditional mutant mice, multiple sets of first arch-like skeletal elements appeared, including partial quadruplication of the jaw cartilage and supernumerary mallei, tympanic, dentary and squamosal bones. We present evidence indicating that such supernumerary elements arose through partial transformation of third and fourth arch post-otic NCC segmental identities. We first show that Hoxa-deleted embryos displayed normal PA segmentation and NCC migration. Subsequently, we document that ectopic jaw-like elements result from a morphological alteration of the greater horn of the hyoid bone and the lateral process of the thyroid cartilage, third and fourth arch derived structures, respectively. Finally, molecular markers normally expressed in the PA1 of wild-type embryos were ectopically induced in the third and fourth PAs of $Wnt1::Cre/Hoxa^{flox/flox}$ mutant specimen. We conclude that in the absence of Hoxa genes in NCCs, the third and fourth arches adopt a partial first arch-like identity, in addition to the homeotic transformation induced in the hyoid arch by the absence of *Hoxa2*. Notably, partial anterior homeotic transformations of PA3 and PA4 were reported in zebrafish that were mutant for the histone acetyltransferase *moz* (monocytic leukemia zinc finger). This mutations is also associated with reduced Hox expression levels (Miller et al., 2004). Altogether, our findings provide strong evidence that post-otic and pre-otic NCCs share the same Hox-free ground patterning program (model in Fig. 6).

Our results revealed an unprecedented role for *Hoxa2*, as well as synergistic interactions between *Hoxa2* and *Hoxa3*, in the patterning of third and fourth PA skeletal derivatives. We have previously shown that *Hoxa2* performs its main patterning role in post-migratory skeletogenic NCCs (Santagati et al., 2005). Given the absence of *Hoxa4* expression in arch 3 and 4 NCCs (see Fig. S1F in the supplementary material) (Behringer et al., 1993), our data imply that the phenotypes obtained in $Wnt1::Cre/Hoxa^{flox/flox}$ mutant embryos can entirely be accounted for by lack of *Hoxa2* and *Hoxa3* in NCCs. However, the role of *Hoxa2* only

becomes apparent in the absence of *Hoxa3*, indicating non-equivalent functions between *Hoxa2* and *Hoxa3*. In the absence of *Hoxa2*, third and fourth arch-derived structures were indeed normally patterned (Rijli et al., 1993), suggesting that *Hoxa3* is able to compensate for the lack of *Hoxa2*. By contrast, in the absence of *Hoxa3*, morphological alterations of hyoid and thyroid cartilages were detected (Chisaka and Capecchi, 1991) showing a prevalent role for *Hoxa3* over *Hoxa2*, in agreement with the posterior prevalence concept (Duboule and Morata, 1994). Homeotic transformations were nevertheless not observed under these conditions. Here, we show that *Hoxa2* function also significantly contributes to patterning the third and fourth arches, as the concomitant removal of *Hoxa2* from a *Hoxa3*-deficient background generated dramatic homeosis.

Because *Hoxa2* and *Hoxa3* have overlapping spatial expression domains in third and fourth arch NCCs (see Fig. S1A,C in the supplementary material), it is nonetheless unclear how third or fourth arch specific patterns can be achieved. *Hoxa2*- or *Hoxa3*-specific functions could result from a difference in their relative expression levels (quantitative difference) and/or target specificity (qualitative difference). In addition, qualitative and/or quantitative differences of expression of other Hox genes in NCCs and/or in PA epithelia may contribute to establish arch specific pattern. Indeed, *Hoxd4* expression overlaps with *Hoxd3* in arch 4 (see Fig. S1E,H,K in the supplementary material). *Hoxd3* is in addition expressed at low levels in subsets of third arch NCCs (see Fig. S1E in the supplementary material) (Manley and Capecchi, 1997) and genetically interacts with *Hoxa3* (Condie and Capecchi, 1994). Such genetic interaction was supported by the deletion of the Hoxd cluster in the context of the conditional inactivation of Hoxa genes in NCCs, resulting in mild thyroid cartilage reduction and occasional fusions to hyoid cartilage (Fig. 2; not shown), and additional ectopic squamosal bones (Fig. 4; supplementary material Table S1).

However, the removal of the *Hoxd* cluster in a NCC-specific Hoxa-deleted background did not increase the extent of the homeotic phenotype by generating, for example, a supernumerary incus (Fig. 2). This might be due to the persistent expressions of *Hoxb2* and *Hoxb3* (see Fig. S4 in the supplementary material; and not shown), although their single or compound deletions were not sufficient to alter third or fourth arch skeletal pattern (Medina-Martinez et al., 2000). Similarly, the *Hoxa2* knockout phenotype was not extended posteriorly by the additional deletion of *Hoxb2* (Davenne et al., 1999), despite its strong expression in third and fourth arches (see Fig. S1B in the supplementary material). Finally, *Hoxa2* and *Hoxa3* expression in the ectoderm and endodermal pouches of third and fourth arches could also have an influence on the patterning of skeletal derivatives. These observations emphasize the specificity of given Hox clusters for strong vertebrate adaptive traits, such as for the limbs or the teguments, as if ancestral genome duplications, which occurred at the base of the vertebrate radiation, had made it possible for Hox clusters to acquire specific roles (Duboule, 2007). In this context, the Hoxa cluster arguably has a primary role in the biology of skeletogenic neural crest cells. More specifically, our data strongly support a pivotal role for *Hoxa3* and *Hoxa2* in patterning third and fourth arch skeletogenic NCCs, whereas Hoxb and Hoxd genes may provide a ‘quantitative backup’, which may become functionally relevant only in the absence of Hoxa genes (see also Rijli and Chambon, 1997).

It is noteworthy that while the duplicated Meckel's (MC2) was always truncated in single *Hoxa2*$^{-/-}$ mutants, it was posteriorly extended and occasionally fully duplicated and fused directly to the MC3 in *Wnt1::Cre/Hoxa*$^{flox/flox}$ newborns (Fig. 2E,F,I,J). This indicates that the absence of *Hoxa3* function in the third PA enhanced the second PA phenotype observed in the *Hoxa2* knockout. In support of this, the inactivation of *Hoxa3* function alone already resulted in a reduction (or an absence) of the lesser horns of the hyoid bone (Chisaka and Capecchi, 1991), a structure of second arch origin. As the expression of *Hoxa3* is not detected in the second PA, *Hoxa3* function can thus influence the patterning of the second arch structures in a non cell autonomous manner, supporting the observation of patterning interactions between neighboring PAs (e.g. Gavalas et al., 1998).

Finally, an important conclusion of this work is that pre-otic and post-otic skeletogenic NCCs may share a common Hox-free ground pattern (model, Fig. 6). In all vertebrates analyzed, including jawless lampreys (Takio et al., 2004), the first mandibular arch is devoid of Hox gene expression, whereas the second arch expresses only PG2 Hox genes. Functional inactivation of PG2 Hox genes in mouse, as well as knockdown approaches in *Xenopus* and zebrafish (Baltzinger et al., 2005; Hunter and Prince, 2002) have revealed that mandibular and hyoid arches share a ground pattern, manifested in the absence of Hox gene function. Accordingly, *Hoxa2* acts as a selector gene by modifying the underlying ground pattern to yield a hyoid specific pattern. Such a proposal was further supported by ectopic Hox PG2 gain-of-function in the first arch of amphibian and bird embryos (Grammatopoulos et al., 2000; Pasqualetti et al., 2000), which was sufficient to elicit the opposite transformation, namely to change mandibular into hyoid identity. These experiments highlighted the wide conservation, throughout vertebrate evolution, of the presumed Hox-free ground pattern between the first two arches.

However, and even though all PAs clearly belong to a metameric series, loss-of-function experiments involving PG3 Hox genes did not allow the assessment of whether or not posterior arch segments share the same ground pattern with the two rostralmost elements of the series. Here, we find that third arch patterning requires functional contributions from both PG3 and PG2 Hox genes, and that in the absence of *Hoxa2* and *Hoxa3* function, third and fourth arch derivatives are partially replaced by jaw-like and other first arch-like structures. This observation thus extends the ground pattern corresponding to the rostralmost element of the metameric series, the mandibular arch, to more posterior segments. In the transition from jawless agnathan to jawed gnathostome vertebrates, the first arch underwent dramatic morphological changes. Our findings indicate that molecular changes that occurred in first arch skeletogenic NCCs and which resulted in a modification of the morphological ground pattern, e.g. the appearance of the jaw, were concomitantly 'built-in' within the second and more posterior arches. Arch-specific Hox codes in turn induced particular morphological changes, thus linking morphological evolution of the mandibular arch to concomitant morphological changes of hyoid and posterior arches.

In the vertebrate hindbrain, the rhombomere ground pattern also corresponds to the rostralmost element of the series, i.e. rhombomere 1, which is devoid of Hox gene activity (Waskiewicz et al., 2002). The finding that hindbrain and PA ground patterns can be modulated by Hox gene functions to select segment-specific morphologies further

underscores the metameric assembly of the pharyngeal region of the vertebrate head. Interestingly, in the short germ band beetle *Tribolium*, the complete deletion of Hox genes resulted in all head, trunk and abdominal embryonic segments acquiring the morphology of the rostralmost segment carrying antennae (Brown et al., 2002). Morphological co-evolution of a metameric series sharing the same ground pattern corresponding to that of the most anterior segment might thus be a rather widespread strategy in animal evolution.

Supplementary Material

Refer to Web version on PubMed Central for supplementary material.

Acknowledgments

We thank M. Poulet for excellent technical assistance, and J. Zakany, A. McMahon (*Wnt1::Cre*) and A. Nagy (*Z/AP*) for mouse lines. We thank M. Schmittbuhl for the statistical analysis. We acknowledge the following colleagues for the generous gift of plasmids: F. Meijlink (*Alx4*), P. Gruss (*Pax1*), J. Drouin (*Pitx1*), J. Cobb (*Hoxd3*), P. Dollé and R. Krumlauf (*Hoxa3*, *Hoxb3*, *Hoxa4*, *Hoxb4*, *Hoxd4*). M. M. was supported by the Faculté de Chirurgie Dentaire de Strasbourg and Ministère de la Recherche. D. D. was supported by funds from the Canton de Genève, the Louis-Jeantet Foundation, the Swiss National Research Fund, the National Center for Competence in Research (NCCR) '*Frontiers in Genetics*' and the EU programs *Cells into Organs* and *Crescendo*. FMR was supported by the Agence Nationale pour la Recherche (ANR), Fondation pour la Recherche Médicale (Equipe labelisée FRM), Association pour la Recherche contre le Cancer (ARC), Association Française contre les Myopathies (AFM), Ministère de la Recherche, by CNRS and INSERM, and by the Novartis Research Foundation.

References

Baltzinger M, Ori M, Pasqualetti M, Nardi I, Rijli FM. Hoxa2 knockdown in Xenopus results in hyoid to mandibular homeosis. Dev Dyn. 2005; 234:858–867. [PubMed: 16222714]

Barrow JR, Capecchi MR. Targeted disruption of the Hoxb-2 locus in mice interferes with expression of Hoxb-1 and Hoxb-4. Development. 1996; 122:3817–3828. [PubMed: 9012503]

Behringer RR, Crotty DA, Tennyson VM, Brinster RL, Palmiter RD, Wolgemuth DJ. Sequences 5′ of the homeobox of the Hox-1.4 gene direct tissue-specific expression of lacZ during mouse development. Development. 1993; 117:823–833. [PubMed: 8100763]

Boulet AM, Capecchi MR. Targeted disruption of hoxc-4 causes esophageal defects and vertebral transformations. Dev Biol. 1996; 177:232–249. [PubMed: 8660891]

Brown SJ, Shippy TD, Beeman RW, Denell RE. Tribolium Hox genes repress antennal development in the gnathos and trunk. Mol Phylogenet Evol. 2002; 24:384–387. [PubMed: 12220981]

Chisaka O, Capecchi MR. Regionally restricted developmental defects resulting from targeted disruption of the mouse homeobox gene hox-1.5. Nature. 1991; 350:473–479. [PubMed: 1673020]

Condie BG, Capecchi MR. Mice with targeted disruptions in the paralogous genes hoxa-3 and hoxd-3 reveal synergistic interactions. Nature. 1994; 370:304–307. [PubMed: 7913519]

Couly G, Grapin-Botton A, Coltey P, Ruhin B, Le Douarin NM. Determination of the identity of the derivatives of the cephalic neural crest: incompatibility between Hox gene expression and lower jaw development. Development. 1998; 125:3445–3459. [PubMed: 9693148]

Creuzet S, Couly G, Le Douarin NM. Patterning the neural crest derivatives during development of the vertebrate head: insights from avian studies. J Anat. 2005; 207:447–459. [PubMed: 16313387]

Crump JG, Swartz ME, Eberhart JK, Kimmel CB. Moz-dependent Hox expression controls segment-specific fate maps of skeletal precursors in the face. Development. 2006; 133:2661–2669. [PubMed: 16774997]

Danielian PS, Muccino D, Rowitch DH, Michael SK, McMahon AP. Modification of gene activity in mouse embryos in utero by a tamoxifen-inducible form of Cre recombinase. Curr Biol. 1998; 8:1323–1326. [PubMed: 9843687]

Davenne M, Maconochie MK, Neun R, Pattyn A, Chambon P, Krumlauf R, Rijli FM. Hoxa2 and Hoxb2 control dorsoventral patterns of neuronal development in the rostral hindbrain. Neuron. 1999; 22:677–691. [PubMed: 10230789]

Duboule D. The rise and fall of Hox gene clusters. Development. 2007; 134:2549–2560. [PubMed: 17553908]

Duboule D, Morata G. Colinearity and functional hierarchy among genes of the homeotic complexes. Trends Genet. 1994; 10:358–364. [PubMed: 7985240]

Gaunt SJ, Krumlauf R, Duboule D. Mouse homeo-genes within a subfamily, Hox-1.4, -2.6 and -5.1, display similar anteroposterior domains of expression in the embryo, but show stage- and tissue-dependent differences in their regulation. Development. 1989; 107:131–141. [PubMed: 2576400]

Gavalas A, Studer M, Lumsden A, Rijli FM, Krumlauf R, Chambon P. Hoxa1 and Hoxb1 synergize in patterning the hindbrain, cranial nerves and second pharyngeal arch. Development. 1998; 125:1123–1136. [PubMed: 9463359]

Gendron-Maguire M, Mallo M, Zhang M, Gridley T. Hoxa-2 mutant mice exhibit homeotic transformation of skeletal elements derived from cranial neural crest. Cell. 1993; 75:1317–1331. [PubMed: 7903600]

Graham A. Deconstructing the pharyngeal metamere. J Exp Zoolog B Mol Dev Evol. 2007; 310:336–344.

Graham A, Heyman I, Lumsden A. Even-numbered rhombomeres control the apoptotic elimination of neural crest cells from odd-numbered rhombomeres in the chick hindbrain. Development. 1993; 119:233–245. [PubMed: 8275859]

Grammatopoulos GA, Bell E, Toole L, Lumsden A, Tucker AS. Homeotic transformation of branchial arch identity after Hoxa2 overexpression. Development. 2000; 127:5355–5365. [PubMed: 11076757]

Horan GS, Ramirez-Solis R, Featherstone MS, Wolgemuth DJ, Bradley A, Behringer RR. Compound mutants for the paralogous hoxa-4, hoxb-4, and hoxd-4 genes show more complete homeotic transformations and a dose-dependent increase in the number of vertebrae transformed. Genes Dev. 1995; 9:1667–1677. [PubMed: 7628700]

Hunter MP, Prince VE. Zebrafish hox paralogue group 2 genes function redundantly as selector genes to pattern the second pharyngeal arch. Dev Biol. 2002; 247:367–389. [PubMed: 12086473]

Kmita M, Tarchini B, Zakany J, Logan M, Tabin CJ, Duboule D. Early developmental arrest of mammalian limbs lacking HoxA/HoxD gene function. Nature. 2005; 435:1113–1116. [PubMed: 15973411]

Kontges G, Lumsden A. Rhombencephalic neural crest segmentation is preserved throughout craniofacial ontogeny. Development. 1996; 122:3229–3242. [PubMed: 8898235]

Kuratani S, Matsuo I, Aizawa S. Developmental patterning and evolution of the mammalian viscerocranium: genetic insights into comparative morphology. Dev Dyn. 1997; 209:139–155. [PubMed: 9186050]

Lanctot C, Moreau A, Chamberland M, Tremblay ML, Drouin J. Hindlimb patterning and mandible development require the Ptx1 gene. Development. 1999; 126:1805–1810. [PubMed: 10101115]

Larsen, WJ. Human Embryology. New York: Churchill Livingstone; 1993.

Lobe CG, Koop KE, Kreppner W, Lomeli H, Gertsenstein M, Nagy A. Z/AP, a double reporter for cre-mediated recombination. Dev Biol. 1999; 208:281–292. [PubMed: 10191045]

Lumsden A, Sprawson N, Graham A. Segmental origin and migration of neural crest cells in the hindbrain region of the chick embryo. Development. 1991; 113:1281–1291. [PubMed: 1811942]

Maden M, Horton C, Graham A, Leonard L, Pizzey J, Siegenthaler G, Lumsden A, Eriksson U. Domains of cellular retinoic acid-binding protein I (CRABP I) expression in the hindbrain and neural crest of the mouse embryo. Mech Dev. 1992; 37:13–23. [PubMed: 1351399]

Manley NR, Capecchi MR. Hox group 3 paralogous genes act synergistically in the formation of somitic and neural crest-derived structures. Dev Biol. 1997; 192:274–288. [PubMed: 9441667]

Medina-Martinez O, Bradley A, Ramirez-Solis R. A large targeted deletion of Hoxb1-Hoxb9 produces a series of single-segment anterior homeotic transformations. Dev Biol. 2000; 222:71–83. [PubMed: 10885747]

Miller CT, Maves L, Kimmel CB. Moz regulates Hox expression and pharyngeal segmental identity in zebrafish. Development. 2004; 131:2443–2461. [PubMed: 15128673]

Oury F, Murakami Y, Renaud JS, Pasqualetti M, Charnay P, Ren SY, Rijli FM. Hoxa2- and rhombomere-dependent development of the mouse facial somatosensory map. Science. 2006; 313:1408–1413. [PubMed: 16902088]

Pasqualetti M, Ori M, Nardi I, Rijli FM. Ectopic Hoxa2 induction after neural crest migration results in homeosis of jaw elements in Xenopus. Development. 2000; 127:5367–5378. [PubMed: 11076758]

Qu S, Li L, Wisdom R. Alx-4: cDNA cloning and characterization of a novel paired-type homeodomain protein. Gene. 1997; 203:217–223. [PubMed: 9426253]

Ramirez-Solis R, Zheng H, Whiting J, Krumlauf R, Bradley A. Hoxb-4 (Hox-2.6) mutant mice show homeotic transformation of a cervical vertebra and defects in the closure of the sternal rudiments. Cell. 1993; 73:279–294. [PubMed: 8097432]

Ren SY, Pasqualetti M, Dierich A, Le Meur M, Rijli FM. A Hoxa2 mutant conditional allele generated by Flp- and Cre-mediated recombination. Genesis. 2002; 32:105–108. [PubMed: 11857791]

Rijli FM, Chambon P. Genetic interactions of Hox genes in limb development: learning from compound mutants. Curr Opin Genet Dev. 1997; 7:481–487. [PubMed: 9309178]

Rijli FM, Mark M, Lakkaraju S, Dierich A, Dolle P, Chambon P. A homeotic transformation is generated in the rostral branchial region of the head by disruption of Hoxa-2, which acts as a selector gene. Cell. 1993; 75:1333–1349. [PubMed: 7903601]

Santagati F, Rijli FM. Cranial neural crest and the building of the vertebrate head. Nat Rev Neurosci. 2003; 4:806–818. [PubMed: 14523380]

Santagati F, Minoux M, Ren SY, Rijli FM. Temporal requirement of Hoxa2 in cranial neural crest skeletal morphogenesis. Development. 2005; 132:4927–4936. [PubMed: 16221728]

Sechrist J, Serbedzija GN, Scherson T, Fraser SE, Bronner-Fraser M. Segmental migration of the hindbrain neural crest does not arise from its segmental generation. Development. 1993; 118:691–703. [PubMed: 7521280]

Shigetani Y, Aizawa S, Kuratani S. Overlapping origins of pharyngeal arch crest cells on the postotic hind-brain. Dev Growth Differ. 1995; 37:733–746.

Sperber SM, Dawid IB. barx1 is necessary for ectomesenchyme proliferation and osteochondroprogenitor condensation in the zebrafish pharyngeal arches. Development. 2008; 321:101–110.

Takio Y, Pasqualetti M, Kuraku S, Hirano S, Rijli FM, Kuratani S. Evolutionary biology: lamprey Hox genes and the evolution of jaws. Nature. 2004; 429:1. p following 262.

Tissier-Seta JP, Mucchielli ML, Mark M, Mattei MG, Goridis C, Brunet JF. Barx1, a new mouse homeodomain transcription factor expressed in cranio-facial ectomesenchyme and the stomach. Mech Dev. 1995; 51:3–15. [PubMed: 7669690]

Trainor PA, Krumlauf R. Hox genes, neural crest cells and branchial arch patterning. Curr Opin Cell Biol. 2001; 13:698–705. [PubMed: 11698185]

Vesque C, Maconochie M, Nonchev S, Ariza-McNaughton L, Kuroiwa A, Charnay P, Krumlauf R. Hoxb-2 transcriptional activation in rhombomeres 3 and 5 requires an evolutionarily conserved cis-acting element in addition to the Krox-20 binding site. EMBO J. 1996; 15:5383–5396. [PubMed: 8895582]

Vieille-Grosjean I, Hunt P, Gulisano M, Boncinelli E, Thorogood P. Branchial HOX gene expression and human craniofacial development. Dev Biol. 1997; 183:49–60. [PubMed: 9119114]

Wallin J, Eibel H, Neubuser A, Wilting J, Koseki H, Balling R. Pax1 is expressed during development of the thymus epithelium and is required for normal T-cell maturation. Development. 1996; 122:23–30. [PubMed: 8565834]

Waskiewicz AJ, Rikhof HA, Moens CB. Eliminating zebrafish pbx proteins reveals a hindbrain ground state. Dev Cell. 2002; 3:723–733. [PubMed: 12431378]

Zakany J, Kmita M, Alarcon P, de la Pompa JL, Duboule D. Localized and transient transcription of Hox genes suggests a link between patterning and the segmentation clock. Cell. 2001; 106:207–217. [PubMed: 11511348]

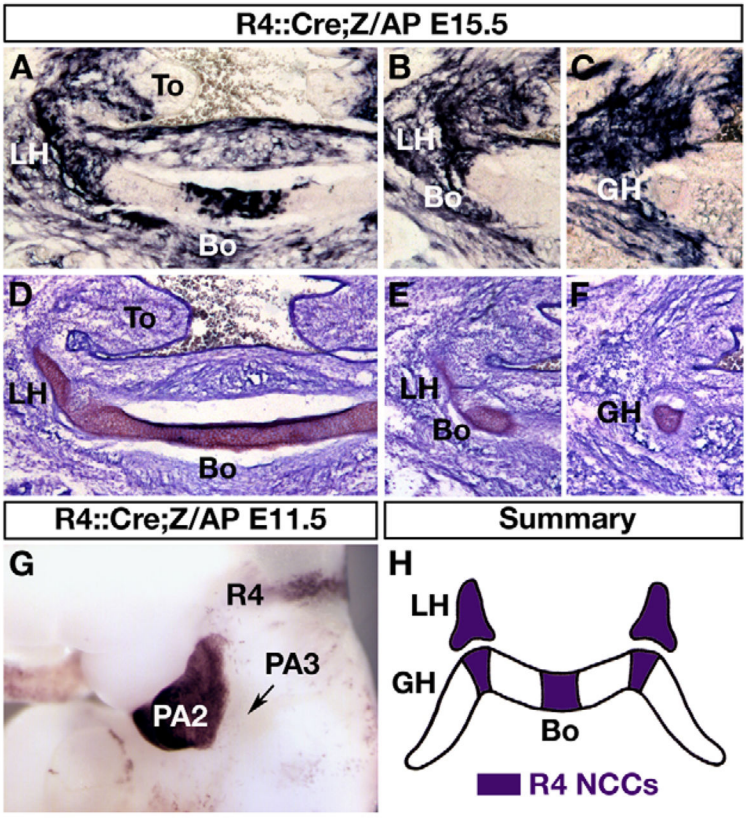

Fig. 1. Pre-otic and post-otic NCC contribution to the hyoid complex

(**A–F**) Alkaline phosphatase (AP) (A–C) and cresyl violet (D–F) staining on adjacent frontal cryosections through the hyoid bone complex of E15.5 *R4::Cre;Z/AP* mouse fetuses. (**G**) Whole-mount AP staining of E11.5 *R4::Cre;Z/AP* mouse embryos. AP is expressed in rhombomere 4 (R4) as well as in PA2 NCCs. PA3 NCCs are devoid of AP expression (arrow). (**H**) Schematic drawing representing the composite origin of the hyoid bone. Rhombomere 4-derived AP+ NCCs contribute to the lesser horns (LH), the central part of the body (Bo) and two symmetrical regions articulating with the lesser horns. The greater horns (GH) are entirely AP negative, thus derived by post-otic NCCs. PA2, second pharyngeal arch; PA3, third pharyngeal arch; To, tongue.

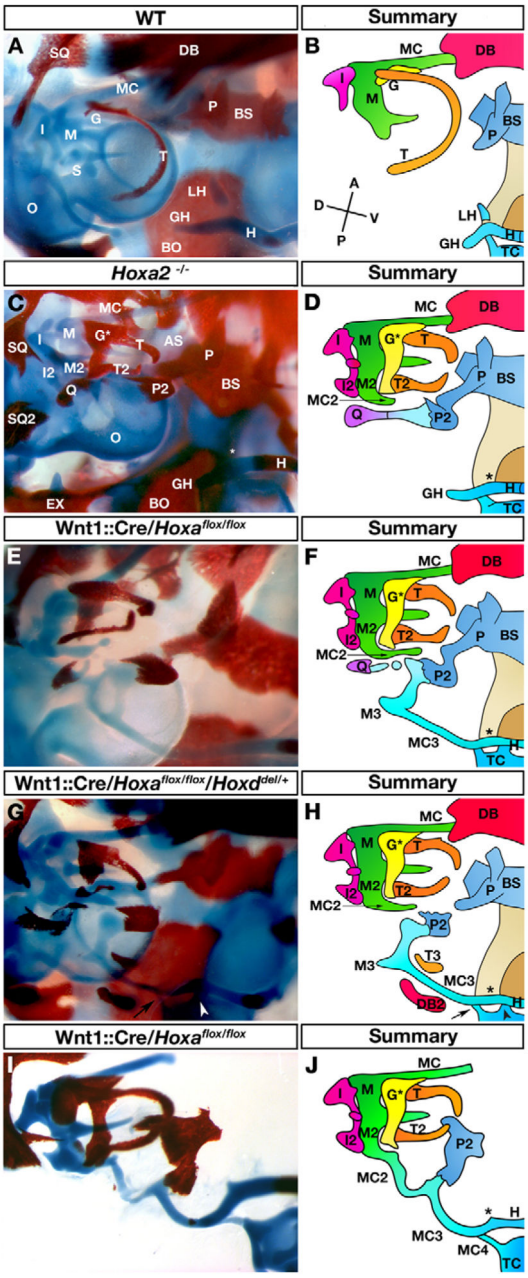

Fig. 2. Homeosis of second, third and fourth arch skeletal derivatives in Hoxa-deleted mouse mutants

(**A–H**) Ventrolateral views of whole-mount head skeletal preparations (A,C,E,G) and their schematic diagrams representing hyoid bone complex, middle ear skeletal elements, dentary bones and skull base elements (B,D,F,H) from wild-type (A,B), *Hoxa2*$^{-/-}$ (C,D), *Wnt1::Cre/Hoxa*$^{flox/flox}$ (E,F) or *Wnt1::Cre/Hoxa*$^{flox/flox}$/*Hoxd*$^{del/+}$ (G,H) newborns. The orientation of the skeletal preparations is shown in B; A, anterior; P, posterior; D, dorsal; V, ventral. (C,D) Homeotic change of PA2 towards PA1 morphology includes absence of styloid process, stapes (S) and lesser horn (LH) of hyoid bone, and appearance of partially duplicated Meckel's cartilage (MC2), incus (I2), malleus (M2), tympanic (T2) and pterygoid (P2)

bones, as well as transformed gonial (G*) and ectopic squamosal (SQ2) bones. (E–H) Additional ectopic skeletal elements are present, indicating homeosis of PA3 and PA4, in addition to PA2, structures towards PA1 morphology. The greater horn (GH) of the hyoid bone is abnormally extended dorsally, resembling a partially triplicated Meckel's cartilage (MC3). MC2 (arrow) is also further extended when compared with D. The dorsal end of MC3 displayed a morphology resembling a supernumerary malleus (M3). In addition, ectopic membranous bone elements near MC3 and M3 may represent supernumerary dentary (DB2) and tympanic (T3) bones. Note that, in order to provide a better magnification for MC3 and M3, SQ2 and SQ3 are outside of the visible field of the picture in E and G. Arrowheads in G,H show fusions between the hyoid and thyroid cartilages. (**I**,**J**) Dissected middle ear and hyoid cartilage elements from a *Wnt1::Cre/Hoxa*$^{flox/flox}$ mutant newborn (I) and their representation in diagram (J). Morphological transformation of the thyroid cartilage (TC) results in an additional ectopic cartilage resembling partial quadruplication of Meckel's jaw cartilage (MC4). Note that MC4 and MC3 directly fuse with an unusually extended MC2, supporting their identity as supernumerary jaw cartilages. (I) The ectopic pterygoid bone (P2) has been dissected out from the basiphenoid (BS) bone. AS, alisphenoid bone; BO, basioccipital bone; DB, dentary bone; EX, exoccipital bone; G, gonial bone; H, hyoid bone; I, incus; M, malleus; MC, Meckel's cartilage; O, otic capsule; P, pterygoid bone; Q, quadrate bone; S, stapes; SQ, squamosal bone; T, tympanic bone. Asterisk indicates absence of lesser horn.

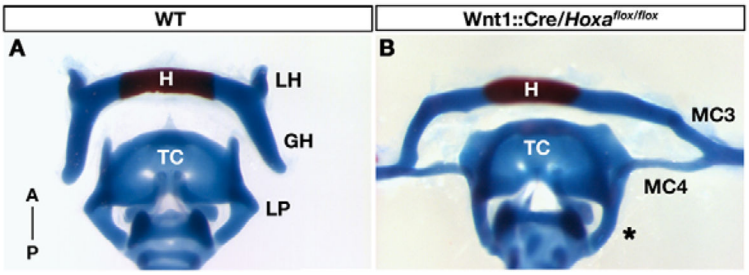

Fig. 3. Transformation of thyroid cartilage into supernumerary jaw element

(**A**,**B**) Frontal view of hyoid (H) and thyroid (TC) skeletal preparations from wild-type (A) and *Wnt1::Cre*/*Hoxa*$^{flox/flox}$ (B) mutant newborns. The orientation of the skeletal preparations is shown in A. (B) Asterisk represents absence of the lateral process (LP) of TC and morphological transformation in an additional ectopic cartilage resembling partial quadruplication of Meckel's jaw cartilage (MC4). Note that MC4 projects dorsally and fuses to a transformed greater horn of the hyoid bone (MC3). LH, lesser horn of hyoid bone; GH, greater horn of hyoid bone.

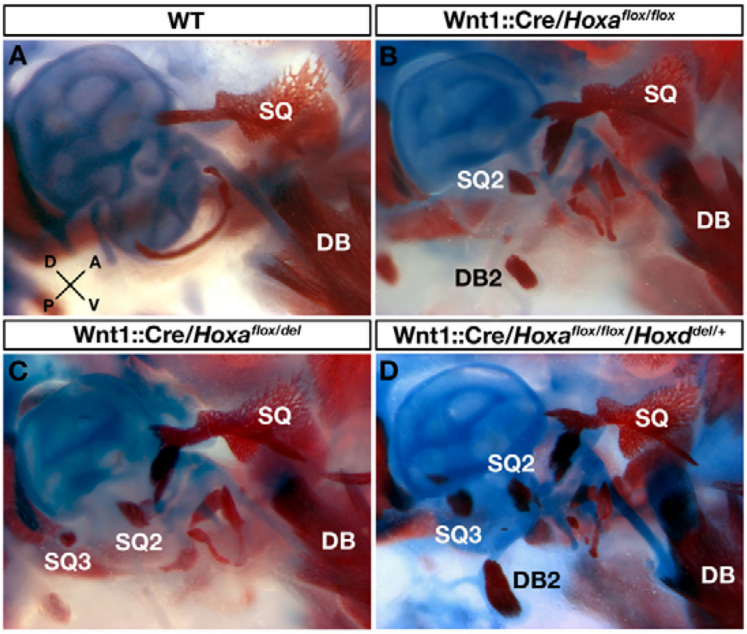

Fig. 4. Ectopic membranous bones in Hoxa and Hoxa/Hoxd deleted mutants

(**A–D**) Lateral views of head skeletal preparations from wild-type (A), *Wnt1::Cre*/*Hoxa*$^{flox/flox}$ (B), *Wnt1::Cre*/*Hoxa*$^{flox/del}$ (C) and *Wnt1::Cre*/*Hoxa*$^{flox/flox}$/*Hoxd*$^{del/+}$ (D) newborns. Orientation is shown in A. Whereas an ectopic partial squamosal bone (SQ2) is a feature of *Hoxa2*$^{-/-}$ mutants (Fig. 2C), additional supernumerary ectopic membranous bones appear in B–D that may reflect partial duplication of dentary (DB2) bone as well as triplication of squamosal (SQ3) bone. DB, dentary bone; SQ, squamosal bone.

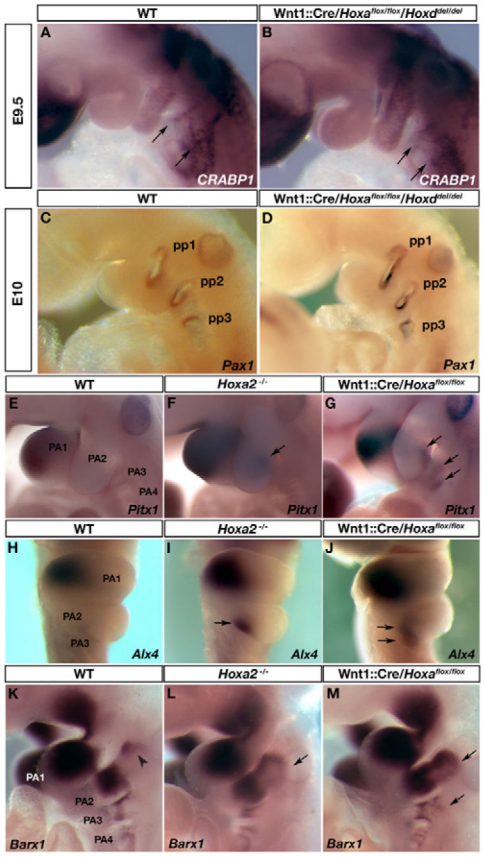

Fig. 5. Molecular changes in Hoxa-deleted embryos support homeosis of post-otic NCCs

(**A–D**) Whole-mount in situ hybridization on wild-type (A,C) and *Wnt1::Cre*/*Hoxa*$^{flox/flox}$/*Hoxd*$^{del/del}$ (B,D) embryos with antisense *CRABP1* (A,B) and *Pax1* (C,D) probes. Arrows show NCC migration into third and fourth pharyngeal arches. *Pax1* expression marks pharyngeal pouches (pp)1-3. Normal NCC migration and arch segmentation is observed in B,D. (**E–M**) Whole-mount in situ hybridization on wild-type (E,H,K), *Hoxa2*$^{-/-}$ (F,I,L) and *Wnt1::Cre*/*Hoxa*$^{flox/flox}$ (G,J,M) E10.5 embryos using antisense *Pitx1* (E–G), *Alx4* (H–J) and *Barx1* (K–M) probes. The arrowhead in K represents a small *Barx1* expression domain at the dorsoanterior margin of PA2. The arrows indicate *Barx1* ectopic expressions in second (PA2), third (PA3), and fourth (PA4) arches. PA1, first pharyngeal arch.

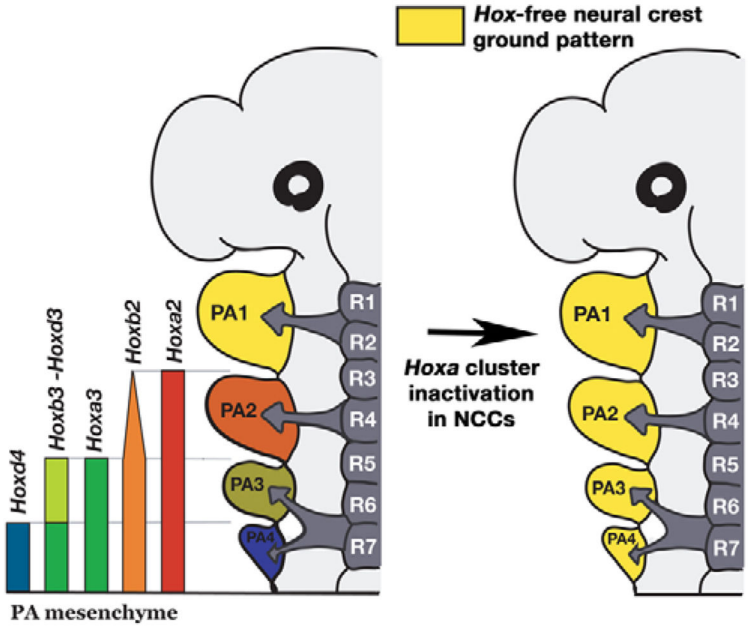

Fig. 6. Hox-free ground pattern for skeletogenic NCC contributing to pharyngeal arches

Vertical colored bars represent Hox gene expression patterns in NCC subpopulations contributing to pharyngeal arch (PA) mesenchyme. On the left side of the drawing, each pharyngeal arch is endowed with a specific Hox expression code represented by a distinct color, with the exception of PA1, which is devoid of Hox expression (yellow). Conditional deletion of Hoxa genes in NCCs reveals that rostral and caudal pharyngeal arches share the same Hox-free ground patterning program corresponding to the mandibular PA1 program. On the right-hand side, all arches are now depicted in yellow.